Journal of Controlled Release 304 (2019) 181–190

Contents lists available at ScienceDirect

Journal of Controlled Release

journal homepage: www.elsevier.com/locate/jconrel

Gene delivery to the rat retina by non-viral vectors based on chloroquine-containing cationic niosomes

Mohamed Mashal[a,1], Noha Attia[a,b,c,1], Gema Martínez-Navarrete[d,e], Cristina Soto-Sánchez[d,e], Eduardo Fernández[d,e], Santiago Grijalvo[d,f], Ramón Eritja[d,f], Gustavo Puras[a,d,*], Jose Luis Pedraz[a,d,*]

[a] NanoBioCel Group, Laboratory of Pharmaceutics, School of Pharmacy, University of the Basque Country (UPV/EHU), Paseo de la Universidad 7, 01006 Vitoria-Gasteiz, Spain
[b] Histology and Cell Biology Department, Faculty of Medicine, University of Alexandria, Alexandria, Egypt
[c] Department of Basic Sciences, The American University of Antigua-College of Medicine, Coolidge, Antigua and Barbuda
[d] Networking Research Centre of Bioengineering, Biomaterials and Nanomedicine (CIBER-BBN), Vitoria-Gasteiz, Spain
[e] Neuroprothesis and Neuroengineering Research Group, Miguel Hernández University, Elche, Spain
[f] Institute of Advanced Chemistry of Catalonia (IQAC-CSIC), Spain

ARTICLE INFO

Keywords:
Niosomes
Non-viral vector
Gene therapy
Retina
Chloroquine

ABSTRACT

The incorporation of chloroquine within nano formulations, rather than as a co-treatment of the cells, could open a new avenue for in vivo retinal gene delivery. In this manuscript, we evaluated the incorporation of chloroquine diphosphate into the cationic niosome formulation composed of poloxamer 188, polysorbate 80 non-ionic surfactants, and 2,3-di (tetradecyloxy) propan-1-amine (hydrochloride salt) cationic lipid, to transfect rat retina. Niosome formulations without and with chloroquine diphosphate (**DPP80**, and **DPP80-CQ**, respectively) were prepared by the reverse phase evaporation technique and characterized in terms of size, PDI, zeta potential, and morphology. After the incorporation of the pCMS-EGFP plasmid, the resultant nioplexes -at different cationic lipid/DNA mass ratios- were further evaluated to compact, liberate, and secure the DNA against enzymatic digestion. In vitro procedures were achieved in ARPE-19 cells to assess transfection efficacy and intracellular transportation. Both nioplexes formulations transfected efficiently ARPE-19 cells, although the cell viability was clearly better in the case of **DPP80-CQ** nioplexes. After subretinal and intravitreal injections, **DPP80** nioplexes were not able to transfect the rat retina. However, chloroquine containing vector showed protein expression in many retinal cells, depending on the administration route. These data provide new insights for retinal gene delivery based on chloroquine-containing niosome non-viral vectors.

1. Introduction

Retinal degeneration is a devastating ocular pathology caused by functional impairment of genes related mainly to the phototransduction process, the structure and metabolism of the retinal cells, and the maturation process of the mRNA needed to synthetize specific proteins. One of the most promising alternatives to treat retinal disorders like age-related macular degeneration [1], Leber congenital amaurosis (LCA) [2] retinitis pigmentosa [3] or choroideremia consists on the delivery of a normal copy of the mutated genes to the affected cells by means of gene therapy technology [4]. Since the success of first RPE65-gene-replacement trials for LCA type-2, further clinical trials of gene therapy have been conducted for other devastating retinal disorders [5]. In most of those clinical trials, viral-vectors have been used to deliver the genetic material. Among them, adeno-associated virus (AAV) stand out for their safety profile [6]. In fact, Luxturna, the first gene therapy-based medicine approved by the FDA in 2017 for the treatment of mutations in RPE65 gene linked to retinitis pigmentosa and Stargardt disease, is based on such AAV. However, the limited carrying capacity of genetic material, around 5 kb, hampers their application to deliver genes that over pass such size to the retina. For instance, ABCA4 and MYO7A genes, whose mutations can be related to Stargardt disease and Usher Syndrome Type 1B, respectively [7], have a size of around 7 kb. Therefore, the use of non-viral vectors represents an

* Corresponding authors at: Laboratory of Pharmacy and Pharmaceutical Technology, School of Pharmacy, University of the Basque Country, 01006 Vitoria-Gasteiz, Spain.
E-mail addresses: gustavo.puras@ehu.eus (G. Puras), joseluis.pedraz@ehu.eus (J.L. Pedraz).
[1] Both authors contributed equally to this work.

https://doi.org/10.1016/j.jconrel.2019.05.010
Received 29 November 2018; Received in revised form 15 February 2019; Accepted 4 May 2019
Available online 06 May 2019
0168-3659/

interesting alternative, since the size of DNA that can be inserted in some of these formulations is theoretically unlimited [8,9].

Despite their limited transfection efficiency and transient gene expression, non-viral vectors have emerged as a promising alternative to deliver genetic material. Some of the main advantages of such gene delivery systems, in addition to their higher carrying capacity, include their low cost of production or their capacity to be easily modified in order to enhance their performance [10,11]. Hence, the research activity related to the design and characterization of novel non-viral vector formulations for gene delivery has considerably increased [12]. Cationic niosomes are self-assembled vesicular nanovehicles, similar to liposomes, with encouraging properties for gene delivery applications. To mention a few, the chemical structure of niosomes makes it possible to provide more stable and less cytotoxic formulations at a low cost [13]. The amphiphilic nature of non-ionic surfactants enable niosomes to trap both hydrophobic and hydrophilic compounds [14].The cationic part here is the hydrochloride salt of the cationic lipid 2,3-di (tetradecyloxy) propan-1-amine (**D**). Such cationic lipid contains the four pivotal components that manage the gene transfection process: a polar head, a backbone, a linker, and two non-polar tails [15].

One of the key limiting steps in the transfection process is the endosomal escape. Chloroquine is a known endosomal disrupting molecule and lysosomotropic agent that can cross the blood retinal barrier. Although chloroquine has been used in vitro as a pre-treatment of cultured cells to facilitate gene delivery [16], this study will be the first -to the best of our knowledge- to apply a chloroquine-containing niosome formulation in gene delivery setting. The incorporation of one or more of the materials at the molecular level, within the nano-formulation, can dramatically affect the transfection process under in vitro and in vivo conditions [12]. Thereafter, scientists may face a great challenge in the near future to test a library of different materials that can be incorporated within the gene delivery vehicles.

Based on the aforementioned (**D**) cationic lipid, two niosome vehicles were formulated for retinal gene delivery with two non-ionic surfactants [polysorbate 80 (**P80**) and poloxamer 188 (**P**)], in the absence/presence of chloroquine (**CQ**), referred as **DPP80** and **DPP80-CQ**, respectively (Fig. 1). The two vehicles were prepared by the emulsification/solvent evaporation system and characterized in terms of particle size, polydispersity index (PDI) and zeta potential. Then, the reporter pCMS-EGFP plasmid was added at different weight ratios of cationic lipid to obtain nioplexes. Such **DPP80/DPP80-CQ** nioplexes were further characterized by size, PDI, charge, morphology, and the capability to compact, liberate and protect the DNA from digestive enzymes. In vitro comparative studies of both vehicles in ARPE-19 cells were achieved respecting their cellular uptake, transfection efficiency, viability and internalization mechanism. Finally, the two formulations were administered to rat eyes via intravitreal and subretinal injections, as a probe of concept, to estimate transfection efficiency by confocal microscopy.

2. Materials and methods

2.1. Production of cationic niosomes

The synthesis of the hydrochloride salt form of the cationic lipid 2,3-di (tetradecyloxy) propan-1-amine (**D**) was performed as described in the literature, with slight modifications of the laboratory protocol [17]. Niosomes were composed by modified reverse-phase evaporation approach [18]. Concisely, 5 mg (0.1% w/v) of the lipid was dispersed in 1 ml of dichloromethane (organic phase). Subsequently, 5 ml milliQ water containing 12.5 mg (0.25% w/v) poloxamer 188 (**P**) (Sigma-Aldrich, Madrid, Spain), 12.5 mg (0.25% w/v) polysorbate 80 (**P80**) (Sigma-Aldrich, Madrid, Spain) and 2.5 mg (0.05% w/v) chloroquine diphosphate (**CQ**) (Sigma-Aldrich, Madrid, Spain) were added to the organic phase. The emulsions were obtained by sonication of the mixture for 50 s at 45 W (Branson Sonifier 250®, Danbury, USA). Dichloromethane was eliminated from emulsions by dissipation under magnetic stirring for 2 h, rendering the cationic niosomes in the aqueous medium. The molar ratios of both **DPP80** and **DPP80-CQ** formulations were, 1.9/0.3/1.9 and 1.9/0.3/1.9/1, respectively.

2.2. Plasmid propagation and elaboration of nioplexes

The protocols for propagation, purification, and quantification of pCMS-EGFP plasmid (5541 bp, Plasmid Factory, Bielefeld, Germany), have been described previously [12]. The nioplexes (niosome/DNA complexes) of both **DPP80** and **DPP80-CQ** were formed by mixing an adequate volume of pCMS-EGFP plasmid stock solution (0.5 mg/ml) with various amounts of the niosome suspension (1 mg cationic lipid/ml) to get different cationic lipid/DNA mass ratios (w/w). To enhance the electrostatic interaction, the nioplexes mixture was allowed to settle for 30 min at room temperature.

2.3. Characterization of niosomes/nioplexes

Dynamic light scattering (DLS) technique was used to estimate both particle size and polydispersity index (PDI) measurements (Malvern Zetasizer Nano ZS, UK). Particle size, was determined by cumulative

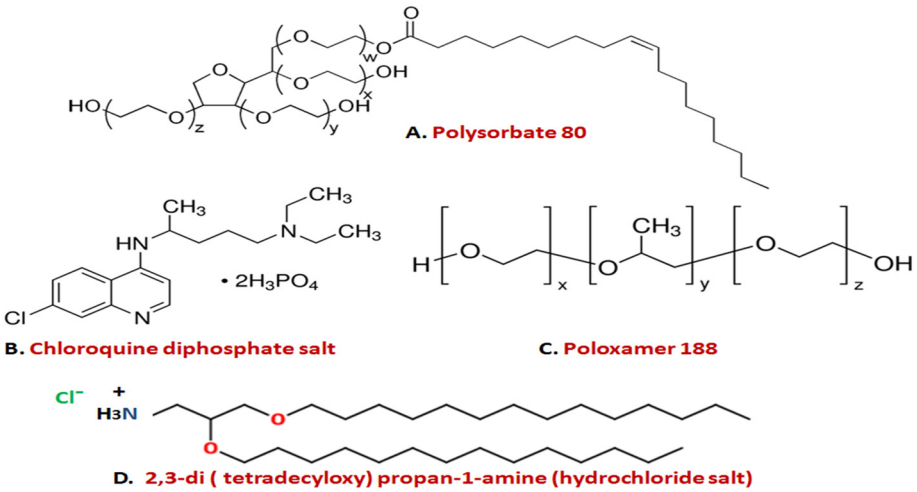

Fig. 1. Chemical structure of the components of **DPP80** and **DPP80-CQ** niosomes. (A) Polysorbate80, (B) Chloroquine diphosphate salt, (C) Poloxamer188 and (D) cationic lipid (DTPA-Cl).

analysis of the recorded hydrodynamic diameter. Laser Doppler Velocimetry (LDV) was used to assess zeta potential (ZP). Samples were dispersed in a 0.1 mM NaCl solution. Triple measurements were carried out for all samples. The morphology of both niosomes and nioplexes was estimated by transmission electron microscopy (TEM). Shortly, onto glow-discharged carbon coated grids, 5 μl sample was allowed to adhere on the surface for 60 s. Samples were examined under TEM, Tecnai G2 20 Twin (FEI, Eindhoven, The Netherlands). In a bright-field image mode, the operation was done with an accelerating voltage of 200 keV. Digital images were captured by an Olympus SIS Morada digital camera. Niosomes' ability to compact, liberate and safeguard DNA from enzymatic digestion was assessed by agarose gel electrophoresis studies. Nioplexes samples (200 mg of plasmid DNA/20 μl) were compared to naked (uncomplexed) DNA. The agarose gel (0.8% w/v) was immersed in a Tris–acetate–EDTA buffer, and the DNA samples were run on the gel for 30 min at 120 V. Next, agarose gel was stained with GelGreen®. A digital ChemiDoc™ MP Imaging System (Bio-Rad, Madrid, Spain) was used for band observation. 20 μl of a 2% SDS solution (Sigma-Aldrich, Madrid, Spain) was added to the samples to estimate the liberation of DNA from both **DPP80** and **DPP80-CQ** vehicles at different cationic lipid/DN mass ratios. In addition, DNase I (Sigma-Aldrich, Madrid, Spain) was added at a concentration of 1 unit of DNase I/2.5 μg DNA to evaluate the protective ability of both vehicles against enzymatic digestion. Then, the samples were incubated at 37 °C for 30 min and a 2% SDS solution was added to evaluate if released the DNA from the vehicles wad protected from the enzymatic digestion.

2.4. In vitro transfection experiments

ARPE-19 cells, purchased from the American Type Culture Collection (ATCC, CRL 2302®), were seeded in 24-well plates at a density of 8×10^4 cells/well, with 500 μl of complete medium, formed of D-MEM/F-12 containing 10% fetal bovine serum (Gibco®, California, USA). Then, at a confluence level of 70–80%, the media was removed, and cells were exposed to nioplexes at different cationic lipid/DNA mass ratios (w/w) (1.25 μg DNA/well) dispersed in serum free Opti-MEM® solution (Gibco®, California, USA) at 37 °C for 4 h. Subsequently, transfection medium was removed, and cells were thoroughly washed 3 times with PBS. Then, cells were cultured in 1 ml of complete medium and allowed to grow for further 72 h until fluorescence microscopy imaging (Nikon TSM) and flow cytometry analysis (FACSCalibur™, BD Biosciences, USA) were done. FL_1 (530/30) was used to detect EGFP-expressing transfected cells, and FL_3 (670) was used to detect Propidium Iodide-stained dead/dying cells. Untransfected cells were used as negative control for all experiments, while cells transfected with Lipofectamine™ 2000 (Invitrogen, California, USA), according to manufacturer's protocol, were considered as positive controls. 10.000-gated events were acquired and analyzed using Flowing Software 2.5.1. Data represent the mean (± SD) of three independent experiments, each of them performed in triplicate.

2.5. Cellular uptake and endocytosis mechanism studies

FITC-labeled (pCMS-EGFP) plasmid (DareBio, Madrid, Spain) was used instead of pCMS-EGFP plasmid to estimate the cellular uptake of the vehicles. The same protocol described in the previous 2.4 section, was used to incubate and maintain ARPE-19 cells, and to evaluate cellular uptake. After removal of the transfection medium and multiple washes of the plates with PBS, the cells were assayed by FACSCalibur flow cytometer. The negative control cells were transfected with naked DNA, and the percentage of FITC-positive cells represented the cellular uptake values. Each specimen was assayed in triplicate. Different uptake inhibitors were used to estimate the endocytosis mechanism of vehicles. Genistein, chlorpromazine hydrochloride, methyl-β-cyclodextrin and wortmannin were used as inhibitors for caveolae-mediated endocytosis (CvME), clathrin-mediated endocytosis (CME), both (CvME and CME) and macropinocytosis (MPC), respectively. Nioplexes at 10/1 cationic lipid/DNA mass ratio were complexed with pCMS-EGFP plasmid, and followed the same protocol described in the previous 2.4 section to transfect ARPE-19 cells. Prior to the addition of nioplexes, cells were incubated with either 200 μM genistein for 30 min, or with 5 mM methyl-β-cyclodextrin, 50 nM wortmannin, or with 5 μg/ml chlorpromazine hydrochloride for 60 min. Cells were incubated with serum-free Opti-MEM® solution for 4 h at 37 °C. Subsequently, cells were carefully washed with PBS after removal of the transfection medium. Then, complete medium was added, and cells were incubated to grow for a further 72 h until flow cytometer analysis was done to determine the transfection efficiency. Each specimen was analyzed in triplicate.

2.6. Buffering capacity of niosomes

The buffering capacity of both **DPP80** and **DPP80-C**Q niosomes was assayed by volumetric analysis. Briefly, 10 ml formulation samples were titrated with aliquots of 100 μl 0.1 M HCl solution, and the changes in pH value were monitored by a pH meter (CRISON, GLP 21, Barcelona, Spain).

2.7. In vivo studies

Intravitreal (4 μl containing 100 ng of pDNA) and subretinal injection (1 μl containing 25 ng of pDNA) of both **DPP80** and **DPP80-CQ** nioplexes suspension were performed into four adult female Sprague–Dawley rats (6–7 weeks old, 200–300 g weight) per formulation. Experiments were done according to the Spanish and European Union regulations for the use of animals in research and the Association for Research in Vision and Ophthalmology (ARVO) statement, as described in the literature [12]. To deliver nioplexes to the subretinal space, a bent 33-gauge needle was introduced through a sclerotomy (1–2 mm) posterior to ora serrata and in a tangential direction toward the posterior retinal pole along the subretinal space. Successful administration was confirmed by the appearance of a partial retinal detachment by direct ophthalmoscopy of the eye fundus through the operating microscope (Zeiss OPMI® pico; Carl Zeiss Meditec GmbH, Jena, Germany). The untreated right eyes were injected only with the vehicles and served as negative controls.

Rats were sacrificed and perfused with 4% paraformaldehyde (PFA) after 72 h and eyes were removed, opened at the cornea and immersed in PFA. For whole mounts, retina was dissected from the eyecup and flattened onto Superfrost glass slides (Superfrost Plus, Fisher Scientific). For cryosections, the eyes were cryoprotected in sucrose and embedded in Tissue-Tek® OCT (optimum cutting temperature). The eyes were cryosectioned at 16 μm and transferred directly onto microscope slides (Superfrost, Fisher Scientific).

For immunohistochemistry, whole mounts or retinal sections were washed and blocked with 10% bovine serum albumine and 0,05% triton in PBS for 1 h (cryosections) or 2 h (whole mounts). Both sections and whole mounts were incubated overnight at 4 °C with primary antibodies: rabbit anti-NeuN (Merck Millipore, MA, USA), rabbit anti-recoverin (Merck Millipore, MA, USA), rabbit anti-Protein kinase C (PKC, Santa Cruz Biotechnology) and rabbit anti-GFAP (Santa Cruz Biotechnology). Samples were rinsed and incubated with Alexa Fluor 555 donkey anti rabbit (Thermofisher Scientific) and counterstained with Hoechst 33342 (Thermofisher Scientific). Finally, whole mounts and sections were mounted with antifade mounting meédium and evaluated with a Leica TCS SPE spectral confocal microscope (Leica Microsystems GmbH, Wetzlar, Germany).

2.8. Statistical analysis

INSTAT program (GraphPad Software, San Diego, CA, USA) was used to perform the statistical analysis. Differences between groups at

Table 1
Physical features of both **DPP80** and **DPP80-CQ** niosomes in terms of size (nm), Polydispersity index (PDI), and zeta potential (mV). The values exemplify the mean ± SD (n = 3).

	Size (nm)	Zeta potential (mV)	PDI
DPP80	90.41 ± 0.65	44.3 ± 1.48	0.42 ± 0.01
DPP80-CQ	118.18 ± 1.46	28.9 ± 7.73	0.13 ± 0.02

significance levels of 95% were calculated by the ANOVA and the Student's t-test. In all cases, P values < .05 were regarded as significant. Normal distribution of samples was assessed by the Kolmogorov-Smirnov test and the homogeneity of the variance by the Levene test. Numerical data were presented as mean ± SD.

3. Results

3.1. Characterization of niosomes/nioplexes

Both niosome vehicles were prepared by mixing [polysorbate 80 (**P80**) and poloxamer 188 (**P**)] non-ionic surfactants and cationic lipid (**D**). In the absence/presence of chloroquine (**CQ**), niosomes were referred as **DPP80,** or as **DPP80-CQ**, respectively (Fig. 1). Both niosomes were prepared by the emulsification/solvent evaporation method and were characterized in terms of particle size, zeta potential (ZP) and polydispersity index (PDI) as shown in Table 1. The incorporation of chloroquine into the **DPP80** niosome formulation increased the size of those niosomes from 90 to118 nm. Moreover, upon chloroquine addition, the ZP values decreased remarkably to 29 mV in **DDP80-CQ** niosomes compared to 44 mV in **DPP80** niosomes. Interestingly, the addition of chloroquine also decreased the PDI value from 0.42 in **DPP80** formulation to 0.13 in **DPP80-CQ** formulation.

Fig. 2 illustrates the physicochemical characterization of **DPP80** and **DPP80-CQ** nioplexes. In Section 2-A, the size and ZP values of both nioplexes at different ratios (from 4/1 to 12/1) can be observed. The size of **DPP80** nioplexes (light bar) generally decreased, with fluctuations, between 170 nm at 4/1cationic lipid/DNA mass ratio to 106 nm at 12/1 mass ratio. With respect to the size of **DPP80-CQ** nioplexes (dark bars), it depicted an evident decreasing pattern (from 300 nm at 4/1 to 140 nm at 12/1 cationic lipid/DNA mass ratios). Basically, the addition of chloroquine to the formulation increased the sizes at all cationic lipid/DNA mass ratios, in comparison to **DPP80** nioplexes. Regarding the ZP, at all cationic lipid/DNA mass ratios, readings of **DPP80** nioplexes (light lines) exceeded their **DPP80-CQ** counterparts (dark lines). Concerning the PDI values (Supplementary data, Table. 1), except for the 4/1 cationic lipid/DNA mass ratio, the PDI values of **DPP80** nioplexes surpassed those of **DPP80-CQ**. As depicted in Fig. 2-B_1, the morphology of **DPP80** nioplexes by TEM, revealed distinct imperfectly spherical structure, while **DPP80-CQ** nioplexes morphology showed aggregated lamellar morphology (Fig. 2-B_2). Fig. 2-C represents the agarose gel electrophoresis assays of both **DPP80** (C_1) and **DPP80-CQ** (C_2) nioplexes prepared at different cationic lipid/DNA mass ratios (4/1, 6/1, 8/1 and 10/1). At all cationic lipid/DNA ratios, both niosomes were able to condense the DNA, since clear white bands were recognized in wells 4, 7, 10, and 13. However, in the case of **DPP80-CQ** (C_2) dim supercoiled (SC) bands were noticed on 7, 10, and 13 wells. Upon SDS addition, the DNA was successfully released from both formulations at all cationic lipid/DNA ratios evaluated, since clear SC bands were observed on lanes 5, 8, 11, and 14. Furthermore, the DNA bound to the surface of both niosome structures was shielded from enzymatic digestion, as clear SC bands were observed on lanes 6, 9, 12, and 15. No SC bands were detected on lane 3, which proves that the plasmid DNA can be fully digested by the DNase I enzyme.

3.2. In vitro transfection and viability studies in ARPE-19 cells

Fig. 3-A depicts the transfection efficiency and cell viability of cationic niosome/DNA nioplexes in ARPE-19 cells. Cationic lipid/DNA mass ratios (w/w) higher than 4/1 showed about 20–30% of cells transfected by both **DPP80** and **DPP80-CQ** nioplexes. However, the

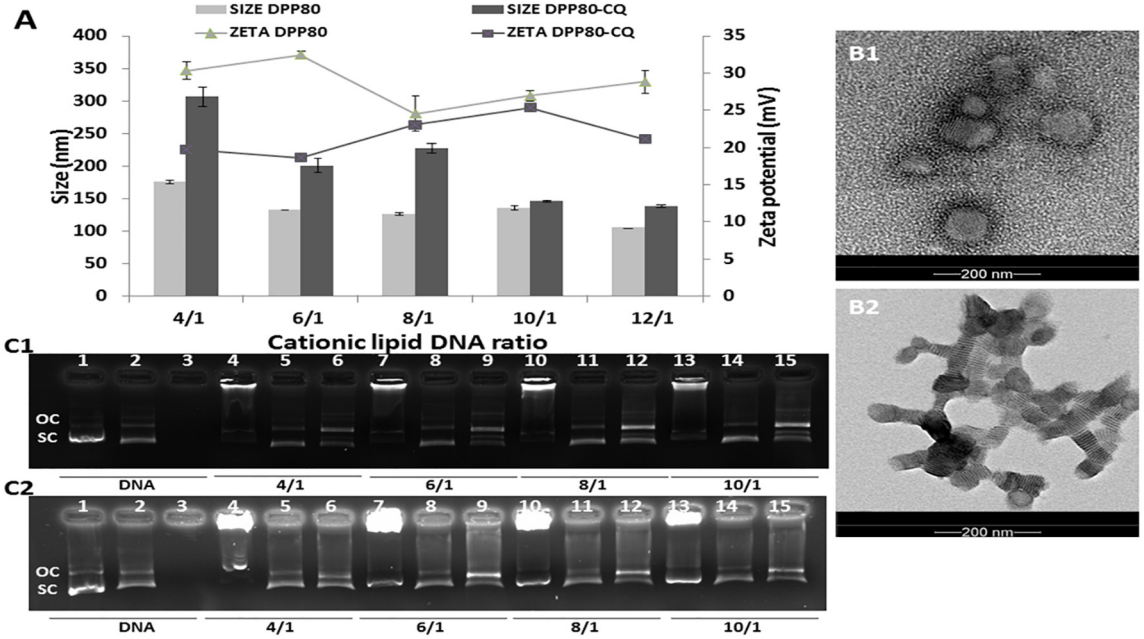

Fig. 2. Physicochemical features of nioplexes. (A) The impact of cationic lipid/DNA mass ratio (w/w) on the size (bars) and zeta potential (lines). The data represent the mean ± SD (n = 3). TEM images of **DPP80** (B_1) and **DPP80-CQ** complexes (B_2) at 8/1 and 10/1cationic lipid/DNA mass ratio (w/w) respectively. Scale bar = 200 nm. (C) condensation, release by SDS and DNase I protection of DNA at various cationic lipid/DNA mass ratios (w/w) of nioplexes based on **DPP80** (C_1) and **DPP80-CQ** (C_2) vehicles depicted by agarose gel electrophoresis. Lanes 1–3 represent uncondensed DNA; lanes 4–6, cationic lipid/DNA mass ratio 4/1; lanes 7–9, cationic lipid/DNA mass ratio 6/1; lanes 10–12, cationic lipid/DNA mass ratio 8/1; lanes 13–15, cationic lipid/DNA mass ratio 10/1. Complexes were processed with SDS (lanes 2, 5, 8, 11 and 14) and DNase I + SDS (lanes 3, 6, 9, 12 and 15). OC: open circular structures, SC: supercoiled structures.

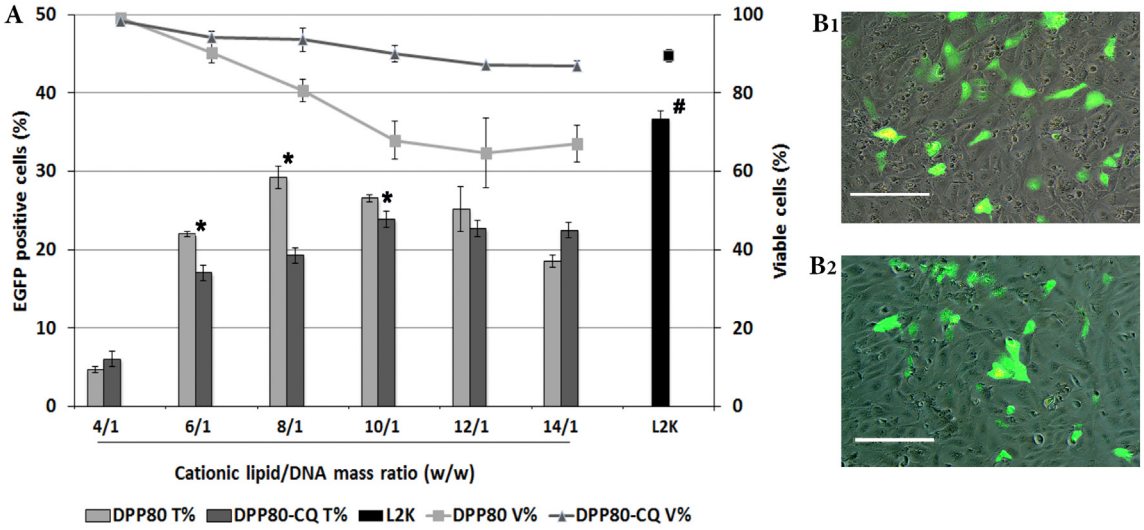

Fig. 3. In vitro transfection and viability performance of both **DPP80** and **DPP80-CQ** nioplexes in ARPE-19 cells. (A) The percentage of EGFP-positive cells (bars) and the percentage of viable cells (lines) at various cationic lipid/DNA mass ratios (w/w) evaluated by flow cytometry at 72 h. Data are expressed in terms of mean ± SD, n = 3. L2K = Lipofectamine™2000. *P < .05 compared to **DPP80**, #P < .05 compared to nioplexes. (B_1 and B_2) fluorescence and phase-contrast overlay micrographs of ARPE-19 cells after 72 h transfection at 8/1 and 10/1 cationic lipid/DNA mass ratios (w/w) for **DPP80** and **DPP80-CQ**, respectively. Scale bar = 100 μm.

values of ARPE-19 cells transfected by **DPP80** nioplexes at 6/1, 8/1 and 12/1 cationic lipid/DNA mass ratios (light bars) were significantly higher that values obtained at those same rations when ARPE-19 were transfected with **DPP80-CQ** (dark bars) formulation. In any case, transfection values for both formulations were significantly lower ($p < .05$) than those values gained with Lipofectamine™2000 (36.6%). Meantime, naked DNA plasmid did not show any transfection (data not shown). Regarding cell viability, all cationic lipid/DNA mass ratios (w/w) studied above 6/1, had obviously revealed higher percentages of viability with **DPP80-CQ** nioplexes compared to their **DPP80** counterparts. The viability value of cells transfected with **DPP80-CQ** at 10/1 cationic lipid /DNA mass ratio (90%) was similar to the viability value obtained with Lipofectamine™ 2000 commercial reagent (89.5%). The micrographs observed in Fig. 3-B_1 for **DPP80**, and in Fig. 3-B_2 for **DPP80-CQ** nioplexes, confirmed the previously mentioned difference in the viability of transfected ARPE- 19 cells with both nioplexes at 8/1 and 10/1 cationic lipid/DNA mass ratios respectively.

3.3. Cellular uptake studies

Fig. 4-A illustrates the cellular uptake study of both **DPP80** and **DPP80-CQ** nioplexes with FITC-labeled pDNA in ARPE-19 cells carried out by flow cytometry. Nioplexes at the cationic lipid/DNA mass ratio of the highest transfection efficiency, 8/1 and 10/1 for **DPP80** and **DPP80-CQ** respectively, were used to evaluate the uptake percentage after 4 h of incubation. The uptake values of **DPP80** and **DPP80-CQ** were 73.60% and 74%, respectively.

3.4. The impacts of endocytosis inhibitors on cellular transfection

Fig. 4-B shows cellular transfection of pCMS-EGFP plasmid, mediated by **DPP80** (light bars) and **DPP80-CQ** (dark bars) nioplexes, in ARPE-19 cells with different endocytosis inhibitors. The transfection results were calculated as percentages from the absolute transfection values obtained by **DPP80** and **DPP80-CQ** nioplexes at 8/1 and 10/1 cationic lipid/DNA mass ratios, respectively, in the absence of endocytosis inhibitors. Transfection efficiency of both nioplexes was slightly affected by the caveolae inhibitor, genistein (transfection values were about 93% for both **DPP80** and **DPP80-CQ**), without statistically significant difference between both nioplexes ($p > 0.05$). Additionally, selective inhibition of CME (by chlorpromazine hydrochloride) had a more pronounced effect on **DPP80** nioplexes than on **DPP80-CQ** ($p < 0.05$) (the normalized values of transfection were 67% and 89%, respectively). Nevertheless, transfection efficiency was more affected by methyl-β-cyclodextrin (inhibitor of both CME and CvME) (transfection values decreased to be 11% and 23% for **DPP80** and **DPP80-CQ** nioplexes without inhibition, respectively). Interestingly, wortmannin, an inhibitor of MPC, had statistically reduced the normalized transfection efficiency of **DPP80-CQ** nioplexes (to be 57%) when compared to **DPP80** counterparts (75%).

3.5. Buffering capacity of niosomes

Fig. 4-C shows the buffering capacity of both **DPP80** and **DPP80-CQ** niosomes. After addition of successive volumes (100 μl) of a 0.1 M HCl aqueous solution to a fixed volume of niosomes (10.000 μl), the pH titration curve revealed that **DPP80-CQ** had a considerably higher buffering capacity than **DPP80**, whereas the initial pH values of both formulations were around 4.

3.6. In vivo study

3.6.1. Histological assessment after subretinal injections

At 10/1 cationic lipid /DNA mass ratio, **DPP80-CQ** nioplexes were administered subretinally. After 72 h, EGFP expression in rat retinae was analyzed by CLSM (Fig. 5). In retinal cross sections, EGFP protein expression was recognized in GCL (Fig. 5-A, and B, white arrows). Interestingly, EGFP expression was also observed in some photoreceptor cells (Fig. 5-A, and C, yellow arrows). Such EGFP expression colocalized with some recoverin positive photoreceptors (Fig. 5-B, yellow arrows). Transfection of **DPP80-CQ** nioplexes on photoreceptors after subretinal adminsitration was also observed on Supplementary Fig. 3 (pink arrows). Additionally, blue arrows observed in Fig. 5-D suggest that some damaged and displaced RPE cells were transfected close to the injection site. It is worth mentioning that no co-localization was observed in the bipolar cells stained with PKC. No fluorescence was detected in the retinae injected with the vehicle (Supplementary Fig. 4-C).

3.6.2. Histological assessment after intravitreal injections

Fig. 6 revealed some EGFP expression in whole mount sections of

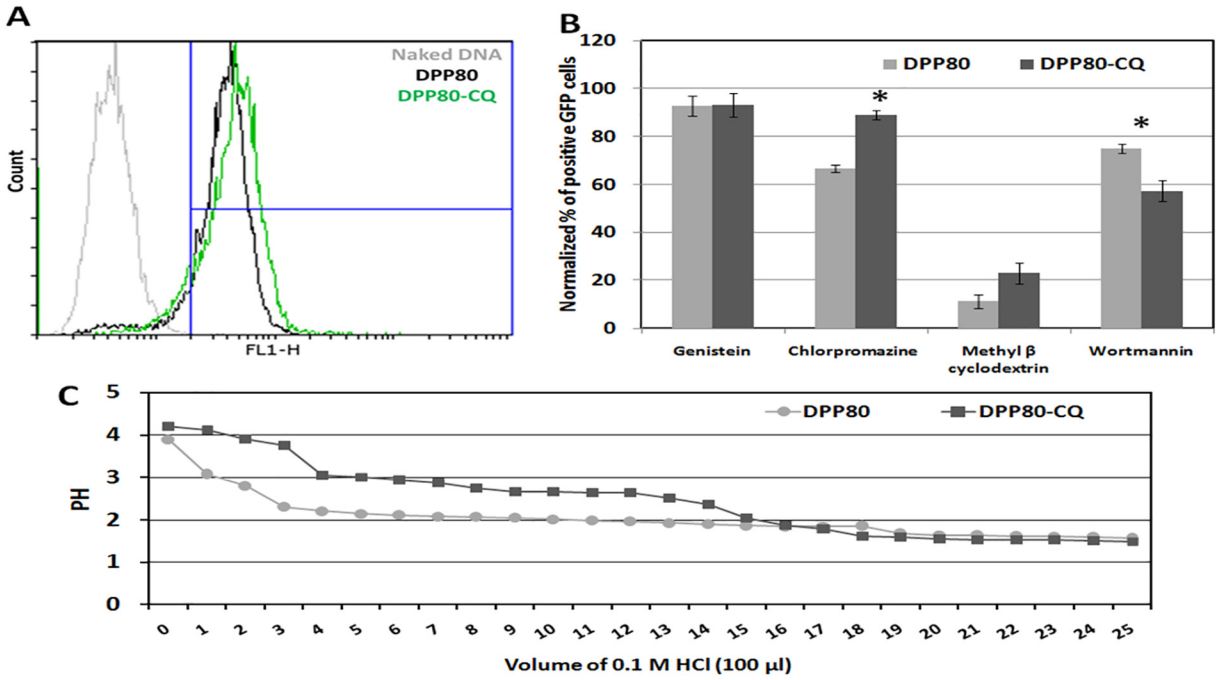

Fig. 4. Cellular uptake and internalization studies of both **DPP80** and **DPP80-CQ** nioplexes at 8/1 and 10/1 cationic lipid/DNA mass ratio. (A) Flow cytometry histograms representing the FITC-labeled plasmid uptake in ARPE-19 cells after 4 h of incubation. (B) Endocytic inhibitors effect on the transfection performance of **DPP80** and **DPP80-CQ** nioplexes. The values were normalized to the transfection without inhibitor. *P < .05 (C) pH buffering capacity analysis of **DPP80** and **DPP80-CQ** niosomes.

the retina in both GCL (Fig. 6-A, white arrows) and INL (Fig. 6-B, yellow arrows), close to the injection site. According to the morphology and the retinal layer examined, such fluorescence could correspond to ganglion and amacrine transfected cells. In any case, endothelial cells migrating to the injection site or glial cells could also have been transfected. Transfection in the GCL was also observed in retinal cross-sections (Fig. 6-D, white arrows) and, interestingly, in the OPL (Fig. 6-C, blue arrows).

After both intravitreal and subretinal injections, we did not observe GFP expression in regions distal from the injection sites (Fig. 4-A, B, Supplementary data).

4. Discussion

In this research work, we offer a novel approach to design, characterize and evaluate chemical vectors for retinal gene delivery. More precisely, we evaluated the role of chloroquine incorporation into niosomes composed of cationic lipid and a mixture of non-ionic surfactants.

Chloroquine, by itself, can enhance transfection efficiency whenever included to the cell culture medium or incorporated into cationic-peptide-DNA complexes [19] in a dose-dependent matter. However, the pre-treatment with chloroquine, has shown high toxicity levels that limit further clinical applications [20]. To avoid such noxious effect, in the current study, chloroquine was incorporated within the niosome formulation. Such inclusion of chloroquine into a niosome formulation, rather than as a co-/pre-treatment of cells, would be a more logical approach for in vivo settings. The amphiphilic nature of both non-ionic surfactants used (**P80** and **P**) can deliver both hydrophilic and lipophilic molecules. Interestingly, propylene oxide chains of the **P** can interact with lipid membranes and induce their structural re-arrangement for better stability and translocation of the gene carriers [21]. In addition, the incorporation of **P** to polycation-DNA complexes enhanced the expression level of the delivered genes in both in vitro and in vivo conditions at doses below the known toxicity levels [22]. **P80** has been reported to act as a co-emulsifier along with **P**, in drug and gene delivery endeavors [23]. Moreover, the encouraging properties of **P80** create a steric barrier that evades the aggregation of nano-vesicles, enhances the cell tolerance [11], and improves transfection efficiency due to the presence of polyethylene glycol (PEG) chains in its structure [24]. However, the ability **P** to form network structures might be more suitable than **P80**, if used with water-soluble cationic lipids, to enhance their flexibility and durability [25]. In such case, a mixture of two specific types of non-tensioactive molecules could provide a synergistic enhancement of nano-vesicle stabilization [26].

Regarding the cationic lipid, the high solubility of the **D**-Cl salt enhances biodistribution of lipid/plasmid complexes, and therefore, transfection efficiency [27]. However, in a previous study, we observed that the solubility of cationic lipid can dramatically shift the transfection results according to the type of the cells and the way of formulation. In that study, the DTPA cationic lipid (non-salt form) succeeded to transfect retinal cells in vitro conditions [11], while in such mentioned study, the salt form failed to transfect retinal cells in vivo. Interestingly, the same formulation with the same salt form of cationic lipid (**DPP80**) succeeded to transfect cerebral cortical cells in vivo [28]. Strikingly, both salt/non-salt forms of the cationic lipid were able to transfect ARPE-19 cells in vitro conditions. In any case, the non-salt form was superior in terms of transfection and cell viability. This contradiction emphasizes the lack of correlation between the in vivo and in vitro transfection conditions and the importance of the formulation at physical level.

To emphasize the impact of chloroquine, **DPP80** and **DPP80-CQ** niosomes were elaborated and compared. The characterization data of both niosomes were analyzed (Table 1). The incorporation of chloroquine slightly increased the size of niosomes by about 28 nm, and reduced both PDI (about 69% decrease) and ZP (about 34% decrease). Drug/gene delivery vehicles are generally favored by small polydispersity values [29]. The positive ZP values (> +25 mV) detected for both niosomes would reflect a potentially long-lasting stability. Once the niosomes were characterized in terms of size, PDI, and zeta potential, nioplexes were elaborated with the pCMS-EGFP plasmid at various cationic lipid/DNA mass ratios by adding the reporter plasmid

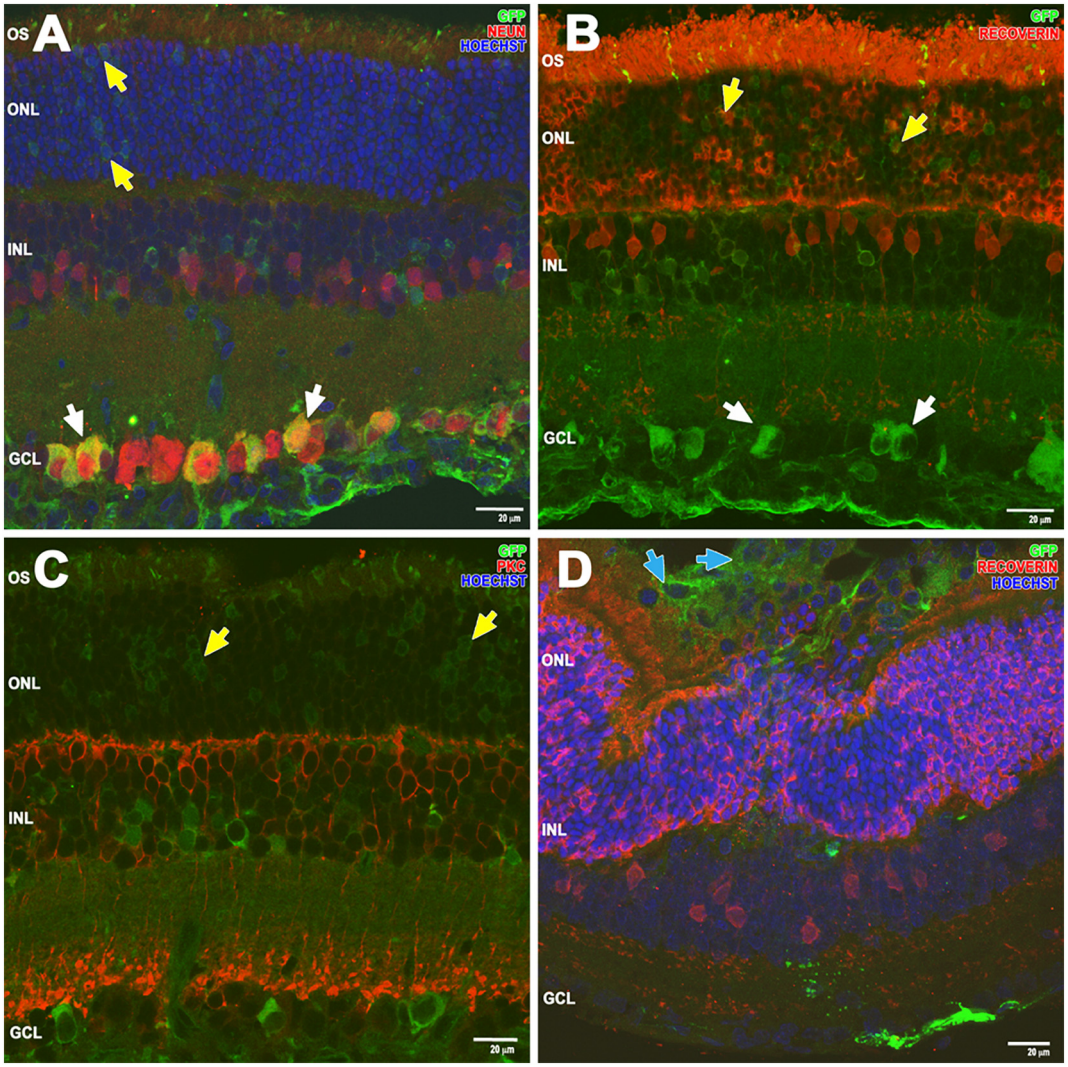

Fig. 5. Retinal cross sections micrographs obtained by confocal microscopy 3 days post subretinal injection of **DPP80-CQ** nioplexes (A–D). EGFP protein was observed mainly in GCL (white arrows), photoreceptors (yellow arrows) and RPE cells (blue arrows). Retinal sections were stained with antibodies against NeuN(A), recoverin (B, D) and protein kinase C (C). The cell nuclei were counterstained with Hoechst 33342. GCL, ganglion cell layer; INL, inner nuclear layer; ONL, outer nuclear layer; OS, photoreceptor outer segment Scale bars: 20 µm. (For interpretation of the references to colour in this figure legend, the reader is referred to the web version of this article.)

to the niosomes and not the opposite to ensure proper condensation process [30]. The ZP of **DPP80** nioplexes was clearly lower when compared to the same niosomes without chloroquine (Fig. 2-A). On the other hand, ZP of chloroquine-containing nioplexes (**DPP80-CQ**) oscillated within a narrower range (19–25 mV) in comparison to **DPP80-CQ** niosomes (29 mV). Generally, the compaction of DNA is improved when 90% of the charge is compensated in an aqueous solution [31]. Strikingly, at 8/1 and 10/1 mass ratios for **DPP80** and **DPP80-CQ**, respectively, ZP values fluctuated within a narrow range (23–27 mV) which represents a small reduction in ZP for **DPP80-CQ** compared to ZP of niosomes (29 mV). This suggests a spontaneous electrostatic interaction of pDNA with **DPP80-CQ** niosomes at 10/1 mass ratio which could be explained by a direct interaction of chloroquine with pDNA. Regarding PDI values of nioplexes, an obvious effect of chloroquine addition at all ratios studied above 4/1 was observed, as PDI values decreased in comparison to **DPP80** formulation (Supplementary Table 1). The electron micrographs illustrated a discrete, almost spherical morphology and absence of aggregates in **DPP80** complexes (Fig. 2-B_1). By contrast, **DPP80-CQ** nioplexes appeared as clusters of multilamellar planar structures that form string-like colloidal aggregates (Fig. 2-B_2). The lamellar spacing was around 5.5–6 nm, suggesting that the pDNA strands were complexed with the cationic lipid bilayers [15]. Similarly, many mixtures of neutral lipids (as DOPC and DOPE), along with cationic lipids (as DOTAP), extensively used for gene delivery purposes, are known to form lamellar complexes with DNA [32].

The agarose gel retardation assay showed that both niosomes, at all studied cationic lipid/DNA ratios, were able to condense, release and protect the DNA from enzymatic digestion (Fig. 2-C). Of note, the relatively lower DNA condensation, observed by the chloroquine-containing formulation (Fig. 2-C_2), did not hamper the release or the protection of the condensed DNA, which is of utmost importance during the transfection process. Any change in condensation efficiency might affect the pattern and topology of spatial DNA configuration. Even more, the state of DNA condensation can be affected by both the type and the content of the surfactant or other additives as chloroquine. Therefore, the fine-tuning of such molecules could be of importance to unveil the mechanism of condensation of different types of DNA molecules within different nano-vesicles. Even at high concentrations of chloroquine, 100 µg/ml, ARPE-19 cells appeared healthy with good viability, despite the appearance of many vacuoles in the cytoplasm (Supplementary Fig. 1). The transfection efficiency in vitro, ARPE-19

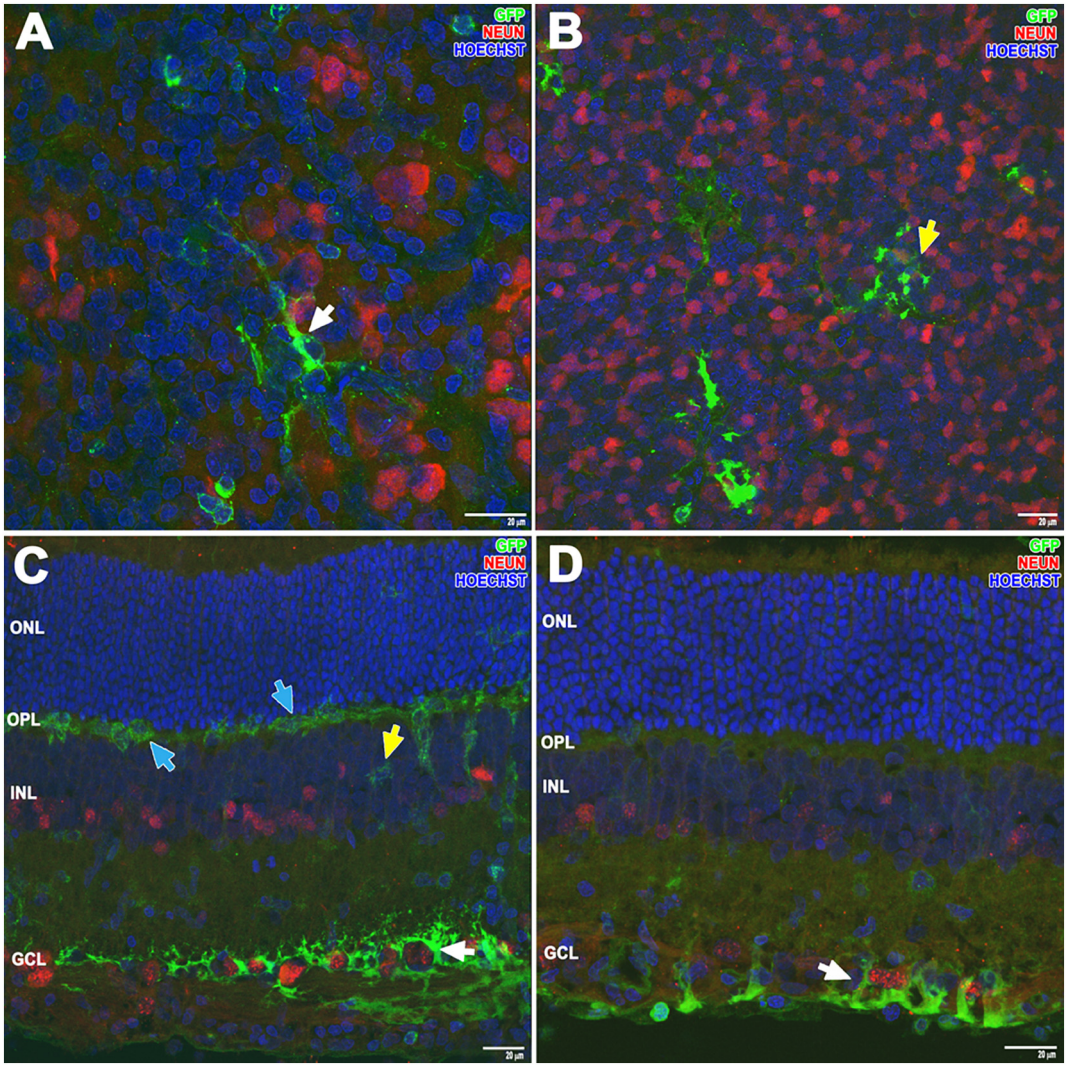

Fig. 6. Confocal fluorescence micrographs of whole mount (A, B) and cross-sections (C, D) of the retina 3 days after intravitreal administration of **DPP80-CQ** nioplexes. EGFP expression can be observed in both GCL (A, C and D, white arrows) and INL (B and C, yellow arrows). Interestingly, some protein expression was also observed in OPL (C, blue arrows). Whole mount and retinal sections were stained with NeuN (A-D). The cell nuclei were counterstained with Hoechst 33342 (blue). GCL, Ganglion cell layer; INL, inner nuclear layer; ONL, outer nuclear layer; OPL, outer plexiform layer. Scale bars: 20 μm. (For interpretation of the references to colour in this figure legend, the reader is referred to the web version of this article.)

cells, fluctuated within a small range in both vectors at all mass ratios studied (Fig. 3). However, the cell viability was in favor of **DPP80-CQ** (Fig. 3-A). Noteworthy, chloroquine inhibits lysosomal enzymes by increasing the pH of the lysosomes and disturbing their fusion with autophagosomes, thus inhibits autophagy [33]. Moreover, chloroquine and its autophagy inhibiting derivative, hydroxychloroquine, are both FDA-approved agents [34]. According to the cell type or the state of stress, autophagy might protect or promote cell death in the eye [35]. This mutable nature of autophagy might be the reason for the increased cell viability observed with **DDP80-CQ** formulation in comparison with its chloroquine-free counterpart, **DPP80**. Generally, cell viability and metabolism of ARPE-19 cells are relatively unaffected by the concentrations of chloroquine between 10 and 30 μg/ml, though affected in a dosage-dependent fashion afterward [36]. To analyze whether the enhanced cell internalization of nioplexes was among the effects that chloroquine could have on niosome formulations, we determined the percentage of ARPE-19 cell uptake of both **DPP80** and **DPP80-CQ** formulations at the mass ratios of best transfection efficiency, 8/1 for **DPP80** and 10/1 for **DPP80-CQ** (Fig. 4). Interestingly, flow cytometry studies showed that chloroquine incorporation had an insignificant effect on the percentage of cellular uptake when compared to the **DPP80** formulation (Fig. 4-A). Such observation is most probably due to the indifferent surface charge of both nioplexes at the aforementioned mass ratios (22.5 ± 7.3 and 25.3 ± 2.5 for **DPP80** and **DPP80-CQ**, respectively, $P > .05$). The similar uptake percentages in such ratios could justify the unaltered transfection results depicted previously (Fig. 3-A). The transfection efficiency can be markedly affected by the mechanism of endocytosis. Consequently, we studied three of the most active cellular internalization pathways: clathrin-mediated endocytosis (CME), caveolae-mediated endocytosis (CvME) and macropinocytosis (MPC). The results observed in Fig. 4-B suggested that **DPP80-CQ** nioplexes were internalized mainly by MPC, while CvME and CME had less participation in the cellular uptake process. Due to its ability to internalize larger structures, macropinocytosis pathway has been proposed to mediate the internalization of non-viral gene delivery vehicles [37]. Moreover, MPC is considered as the major pathway responsible for DNA transfection in certain cell types [38]. In contrary, **DPP80** nioplexes were internalized mainly by CME and, to a lesser extent, by MPC, while CvME had a much less participation in the cellular uptake process. However, the minor fluctuation in transfection efficiency between the two nioplexes could be due to limited variations between the two main different mechanisms of internalization (CME for

DPP80 and MPC for **DPP80-CQ**). The delivery of genetic material by CvME and CME passes through late endosomes/lysosomes, which increases the hazards of DNA degradation and lowers the transfection efficiency [39]. So, an expected trivial effect of CvME and especially CME pathways could explain the high percentages of EGFP expression in ARPE cells by both nioplexes (Fig. 3), compared to lipofectamine® 2000 (approximately, 80% and 75% of lipofectamine®2000 for **DPP80** and **DPP80-CQ**, respectively).

Afterwards, we analyzed the pH-buffering capacity of both niosomes (Fig. 4-C). The incorporation of chloroquine into the niosome formulation increased the pH-buffering capacity upon titration with 0.1 M HCl, compared to the niosomes elaborated without chloroquine (at pH values > 2). Though, there was no change in the buffering capacity when the pH was < 2 for both niosomes. Chloroquine might induce endosomal and lysosomal escape via the proton sponge effect [40]. This result could suggest that chloroquine-containing formulation could increase the proton sponge effect, and therefore, the endosomal escape capacity of **DPP80-CQ** niosomes. However, as the predominant mechanism of internalization for **DPP80-CQ** was neither CvME nor CME, the impact of the proton sponge effect of chloroquine on the transfection efficiency was insignificant.

Based on the previously mentioned physicochemical and in vitro biological results, we were enthusiastic to perform a preliminary in vivo study to evaluate the transfection efficiency of our formulations, **DPP80-CQ** in particular, in rat retinae after both subretinal (Fig. 5), and intravitreal injections (Fig. 6). Subretinal injection is a well-known clinical route to deliver genetic/drug material to the back of the eye. In addition, it enables direct contact of the injected nucleic acids with the outer retinal layers, photoreceptors and RPE cells. Noteworthy, clinical trials to treat many inherited retinal diseases such as LCA type 2 used the subretinal injection route [41]. However, it is less desirable than the intravitreal route due to the possible complications; such as retinal detachment or the localized side effects around the site of injection. Generally, IV injection is more widely applicable in the clinical practice due to its ability to deliver genetic material to a larger retinal surface, in addition to less surgical trauma compared to the SR route [42].

Surprisingly, **DPP80** did not induce any transfection to retinal cells in vivo after both subretinal or intravitreal injections (Supplementary Fig. 2), whereas the chloroquine-containing formulation, **DPP80-CQ** did (Figs. 5 and 6). The lack of correlation between in vitro and in vivo transfection results has been widely reported as it is a context-dependent matter [12].

Based on previous physicochemical and in vitro biological results, we were enthusiastic to perform a preliminary in vivo study to evaluate the transfection efficiency of our formulations, **DPP80-CQ** in particular, in rat retinae after subretinal (Fig. 5) and intravitreal injections (Fig. 6). Subretinal injection is a well-known clinical viable route to deliver genetic material to the eye. It enables direct contact of the injected nucleic acids with the outer retinal layers, photoreceptors and RPE cells. Noteworthy, clinical trials to treat many inherited retinal diseases such as LCA type 2 use subretinal injection [41]. However, it is less desirable than the IV route due to the possible complications such as retinal detachment or the localized effect around the site of injection. Generally, intravitreal injection is more widely applicable in the clinical practice due to its ability to deliver genetic materials to a larger retinal surface and advantages of less surgical trauma compared to the SR route [42].

Subretinal administration allows direct contact of genetic material with RPE cells and outer layer of the retina. Although this route of administration is highly effective to locally transfect cells close to the site of the injection, the occasionally observed side effects, related to this invasive route, such as retinal detachment, hemorrhages or alterations in RPE cells can hamper its practice [43]. In any case, subretinal injections have been widely used on clinical trials to treat some devastating genetic disorders of the retina reporting excellent outcomes [44]. In addition, the recently FDA/EMA-approved Luxturna medicine to deliver healthy copies of the RPE65 gene to the retina is administered by subretinal injection. In our in vivo experiments, after subretinal administration of nioplexes, we observed localized EGFP expression, mainly in some photoreceptor and RPE cells, close to the injection site. Transfection at this level can have clinical relevance because mutations of > 200 genes in RPE cells/photoreceptors are related to relevant genetic disorders of the retina such as; Leber congenital amaurosis, retinitis pigmentosa, and Stargardt disease, to name just a few ones [45].

Compared to subretinal injection, intravitreal injection represents an interesting alternative to deliver genetic material to the back of the eye, and therefore to access retinal structure. It is a less invasive route, more easily to perform, and higher doses can be delivered [46]. Consequently, large retinal surfaces can be transfected by this route of administration [47]. When we administered 4 μl of **DPP80-CQ** nioplexes by intravitreal injection, the inner layers of the retina (GCL and INL) were mainly transfected as observed in Fig. 6. (white and yellow arrows, respectively). Transfection at this level can be of clinical relevance in treatment of devastating ocular pathologies that compromise the function of ganglion cells as glaucoma [48]. Interestingly, EGFP expression was also discerned in the OPL (Fig. 6-C, blue arrows) which suggests that nioplexes partially diffused, not only through the vitreous where they were administered, but also through the inner retinal layers until reach the OPL. Transfection of the outer layers of the retina by intravitreal administration of non-viral vectors represents a great challenge for the scientific community, since can avoid the subretinal injections and the corresponding side effects commonly associated to such injection.

Unfortunately, chloroquine, like other endolytic agents, has been found to be cytotoxic in several pre-clinical or clinical trials [49]. Chloroquine passes the blood-retinal barrier and is toxic to the retina. Nevertheless, such retinal toxicity is related to large doses and long-term use of chloroquine [50]. In this study, at 10/1 cationic lipid /DNA mass ratio, the final concentration of chloroquine was only 25 μg/ml which did not induce any significant cytotoxicity in accordance with Chen et al, [36]. The affinity of retinal cells to the modified salt form of the cationic lipid, in addition to the favorable properties of **P** and **P80**, along with the effect of chloroquine, raise the possibility to target different retinal cell layers safely and effectively after both subretinal and intravitreal administrations.

5. Conclusions

The addition of chloroquine to a niosome formulation retained its functionality in vitro, but most importantly, enhanced its transfection ability in vivo. This work highlights the use of chloroquine as a built-in component in the gene delivery vehicles to evade its toxicity and to provide new insights into the future of retinal gene therapy.

Acknowledgements and disclosures

This project was supported by the Basque Country Government (CGIC10/172), Spanish Ministry of Education (Grant CTQ2017-84415-R, MAT2015-69967-C3-1R), the Generalitat de Catalunya (2014/SGR/624) and the Instituto de Salud Carlos III (CB06_01_0019, CB06_01_1028). The authors also wish to thank the intellectual and technical assistance from the ICTS “NANBIOSIS”, more specifically by the Drug Formulation Unit (U10) of the CIBER in Bioengineering, Biomaterials, and Nanomedicine (CIBER-BBN) at the University of Basque Country (UPV/EHU). Technical and human support provided by SGIker (UPV/EHU) is acknowledged.

Appendix A. Supplementary data

Supplementary data to this article can be found online at https://doi.org/10.1016/j.jconrel.2019.05.010.

References

[1] I.J. Constable, et al., Gene therapy for age-related macular degeneration, Asia Pacific J. Ophthalmol. 5 (4) (2016) 300–303.
[2] A.M. Maguire, et al., Age-dependent effects of RPE65 gene therapy for Leber's congenital amaurosis: a phase 1 dose-escalation trial, Lancet 374 (9701) (2009) 1597–1605.
[3] W.A. Beltran, et al., Gene therapy rescues photoreceptor blindness in dogs and paves the way for treating human X-linked retinitis pigmentosa, Proc. Natl. Acad. Sci. 109 (6) (2012) 2132–2137.
[4] K. Balaggan, R. Ali, Ocular gene delivery using lentiviral vectors, Gene Ther. 19 (2) (2012) 145.
[5] A.M. Maguire, et al., Safety and efficacy of gene transfer for Leber's congenital amaurosis, N. Engl. J. Med. 358 (21) (2008) 2240–2248.
[6] M.F. Naso, et al., Adeno-Associated Virus (AAV) as a Vector for Gene Therapy, 31(4) (2017), pp. 317–334.
[7] D.J. Jiang, C.L. Xu, S.H.J.G. Tsang, Revolution in Gene Medicine Therapy and Genome Surgery, 9(12) (2018), p. 575.
[8] M. Agirre, et al., Delivery of an Adenovirus Vector Plasmid by Ultrapure Oligochitosan Based Polyplexes, 479(2) (2015), pp. 312–319.
[9] M. Mashal, et al., Non-viral Vectors Based on Cationic Niosomes as Efficient Gene Delivery Vehicles to Central Nervous System Cells into the Brain, 552(1–2) (2018), pp. 48–55.
[10] R. Zulliger, et al., Optimizing Non-viral Gene Therapy Vectors for Delivery to Photoreceptors and Retinal Pigment Epithelial Cells, in Retinal Degenerative Diseases, Springer, 2018, pp. 109–115.
[11] G. Puras, et al., A novel cationic niosome formulation for gene delivery to the retina, J. Control. Release 174 (2014) 27–36.
[12] M. Mashal, et al., Retinal gene delivery enhancement by lycopene incorporation into cationic niosomes based on DOTMA and polysorbate 60, J. Control. Release 254 (2017) 55–64.
[13] S. Grijalvo, et al., Cationic Niosomes as Non-Viral Vehicles for Nucleic Acids: Challenges and Opportunities in Gene Delivery, 11(2) (2019), p. 50.
[14] G.P. Kumar, P. Rajeshwarrao, Nonionic surfactant vesicular systems for effective drug delivery—an overview, Acta Pharm. Sin. B 1 (4) (2011) 208–219.
[15] N. Attia, et al., Stem cell-based gene delivery mediated by cationic niosomes for bone regeneration, Nanomedicine 14 (2) (2018) 521–531.
[16] P. Erbacher, et al., Putative role of chloroquine in gene transfer into a human hepatoma cell line by DNA/lactosylated polylysine complexes, Exp. Cell Res. 225 (1) (1996) 186–194.
[17] G. Kokotos, R. Verger, A. Chiou, Synthesis of 2-oxo amide triacylglycerol analogues and study of their inhibition effect on pancreatic and gastric lipases, Chem. Eur. J. 6 (22) (2000) 4211–4217.
[18] E. Ojeda, et al., Elaboration and Physicochemical Characterization of Niosome-Based Nioplexes for Gene Delivery Purposes, in Non-Viral Gene Delivery Vectors, Springer, 2016, pp. 63–75.
[19] S. Yang, et al., Cellular uptake of self-assembled cationic peptide–DNA complexes: multifunctional role of the enhancer chloroquine, J. Control. Release 135 (2) (2009) 159–165.
[20] X. Zhang, et al., The in vivo use of chloroquine to promote non-viral gene delivery to the liver via the portal vein and bile duct, J. Gene Med. 5 (3) (2003) 209–218.
[21] M. Morille, et al., Progress in developing cationic vectors for non-viral systemic gene therapy against cancer, Biomaterials 29 (24–25) (2008) 3477–3496.
[22] S. Sriadibhatla, et al., Transcriptional activation of gene expression by pluronic block copolymers in stably and transiently transfected cells, Mol. Ther. 13 (4) (2006) 804–813.
[23] A.V. Kabanov, E.V. Batrakova, V.Y. Alakhov, Pluronic® block copolymers as novel polymer therapeutics for drug and gene delivery, J. Control. Release 82 (2–3) (2002) 189–212.
[24] H. Lee, J.H. Jeong, T.G. Park, PEG grafted polylysine with fusogenic peptide for gene delivery: high transfection efficiency with low cytotoxicity, J. Control. Release 79 (1–3) (2002) 283–291.
[25] C. Freitas, R.H. Müller, Effect of light and temperature on zeta potential and physical stability in solid lipid nanoparticle (SLN™) dispersions, Int. J. Pharm. 168 (2) (1998) 221–229.
[26] McGregor, W.C., J. Stubstad, and C.P. Chang, Pharmaceutical compositions of bactericidal/permeability increasing protein (BPI). 2000, Google Patents.
[27] R.I. Mahato, Water insoluble and soluble lipids for gene delivery, Adv. Drug Deliv. Rev. 57 (5) (2005) 699–712.
[28] N. Attia, et al., Gene Transfer to Rat Cerebral Cortex Mediated by Polysorbate 80 and Poloxamer 188 Nonionic Surfactant Vesicles, (2018).
[29] N. Nafee, et al., Chitosan-coated PLGA nanoparticles for DNA/RNA delivery: effect of the formulation parameters on complexation and transfection of antisense oligonucleotides, Nanomedicine 3 (3) (2007) 173–183.
[30] L. Wasungu, D. Hoekstra, Cationic lipids, lipoplexes and intracellular delivery of genes, J. Control. Release 116 (2) (2006) 255–264.
[31] F. Ke, et al., Characterizing DNA condensation and conformational changes in organic solvents, PLoS One 5 (10) (2010) e13308.
[32] J.O. Rädler, et al., Structure of DNA-cationic liposome complexes: DNA intercalation in multilamellar membranes in distinct interhelical packing regimes, Science 275 (5301) (1997) 810–814.
[33] P. Maycotte, et al., Chloroquine sensitizes breast cancer cells to chemotherapy independent of autophagy, Autophagy 8 (2) (2012) 200–212.
[34] S. Zhou, et al., Autophagy in tumorigenesis and cancer therapy: Dr. Jekyll or Mr. Hyde? Cancer Lett. 323 (2) (2012) 115–127.
[35] S.-J. Sheu, et al., Differential autophagic effects of vital dyes in retinal pigment epithelial ARPE-19 and photoreceptor 661W cells, PLoS One 12 (3) (2017) e0174736.
[36] P.M. Chen, Z.J. Gombart, J.W. Chen, Chloroquine treatment of ARPE-19 cells leads to lysosome dilation and intracellular lipid accumulation: possible implications of lysosomal dysfunction in macular degeneration, Cell Biosci. 1 (1) (2011) 10.
[37] C.M. Wiethoff, C.R. Middaugh, Barriers to nonviral gene delivery, J. Pharm. Sci. 92 (2) (2003) 203–217.
[38] X.-X. Zhang, P.G. Allen, M. Grinstaff, Macropinocytosis is the major pathway responsible for DNA transfection in CHO cells by a charge-reversal amphiphile, Mol. Pharm. 8 (3) (2011) 758–766.
[39] S. Xiang, et al., Uptake mechanisms of non-viral gene delivery, J. Control. Release 158 (3) (2012) 371–378.
[40] L.D. Cervia, et al., Distinct effects of endosomal escape and inhibition of endosomal trafficking on gene delivery via electrotransfection, PLoS One 12 (2) (2017) e0171699.
[41] J. Bennett, et al., AAV2 gene therapy readministration in three adults with congenital blindness, Sci. Transl. Med. 4 (120) (2012) (p. 120ra15-120ra15).
[42] H. Koo, et al., The movement of self-assembled amphiphilic polymeric nanoparticles in the vitreous and retina after intravitreal injection, Biomaterials 33 (12) (2012) 3485–3493.
[43] C. Bloquel, et al., Non-viral Ocular Gene Therapy: Potential Ocular Therapeutic Avenues, 58(11) (2006), pp. 1224–1242.
[44] Y. Peng, L. Tang, Y. Zhou, Subretinal Injection: A Review on the Novel Route of Therapeutic Delivery for Vitreoretinal Diseases, Ophthalmic Res. 58 (2017) 217–226.
[45] M. Hims, S. Daiger, C. Inglehearn, Retinitis pigmentosa: genes, proteins and prospects, Genetics in Ophthalmology, Karger Publishers, 2003, pp. 109–125.
[46] A. del Pozo-Rodríguez, et al., Applications of Lipid Nanoparticles in Gene Therapy, 109 (2016), pp. 184–193.
[47] P. Dureau, et al., Quantitative Analysis of Subretinal Injections in the Rat, 238(7) (2000), pp. 608–614.
[48] A. Bosco, et al., Complement C3-Targeted Gene Therapy Restricts Onset and Progression of Neurodegeneration in Chronic Mouse Glaucoma, 26(10) (2018), pp. 2379–2396.
[49] P. Lönn, et al., Enhancing endosomal escape for intracellular delivery of macromolecular biologic therapeutics, Sci. Rep. 6 (2016) 32301.
[50] N. Kasturi, Long-term continuation of chloroquine-induced retinal toxicity in rheumatoid arthritis despite drug cessation, Rheumatology 55 (4) (2015) 766–768.